Bond graph modeling is an attractive means of modeling a dynamic physical system [21,22]. It uses a language based on power exchange within a system model where the structure of the system model is shown graphically [23]. One of the most interesting advantages of bond graph modeling is that it can efficiently represent analytical models graphically in complicated cases involving the coupling of multiple energy domains (*i.e.,* mechanical, electrical, hydraulic, thermal, or magnetic domains) [24-28].

4.2. Thermal domain modeling

Conventionally, a thermal system is analogous to electricity: that is, temperature is similar to voltage and the heat flow rate is similar to a current. A thermal domain system can therefore be represented by thermal resistance and thermal capacitance in a thermal network. The model was developed using the commercial program 20-Sim available through Controllab B.V. [29].

Figure 13(a) shows an equivalent thermal network model of the heat flow inside of the fluid channel based on 2D transient modeling; Figure 13(b) shows a bond graph model of the fluid channel part. The heat from the objective fluid flow inside the fluid channel and some of heat that flows to the developed sensor part and elsewhere flows simultaneously to the ambient. Heat loss caused by radiation is not considered due to the low temperature of fluid. Heat loss caused by convection and conduction can affect the result, so thermal resistance can be obtained from the real experiments. If the temperature between fluid on sensitive area and sensor surface is acquired, thermal resistance containing both convection and conduction can be calculated. However, thermal resistance and heat capacity of sensor part can be calculated from its material properties and geometry [30]. Figure 14 shows the bond graph model of the sensor part and values. The heat generated by the heater flows to the fluid channel through the passivation layer and the thermopile structure. The heat generated from the fluid channel flows to the thermopile structure and to the micro calibration heater. The sensor modeling part consists of a micro calibration heater for characterization of the sensor, a thermopile structure for measurement, a fluid channel model for microfluidic application, and a sourcemeter and the heater modulator for the thermal modulation method.

Figure 13. (a) Heat flow model of a fluid channel; (b) bond graph model of a fluid channel.

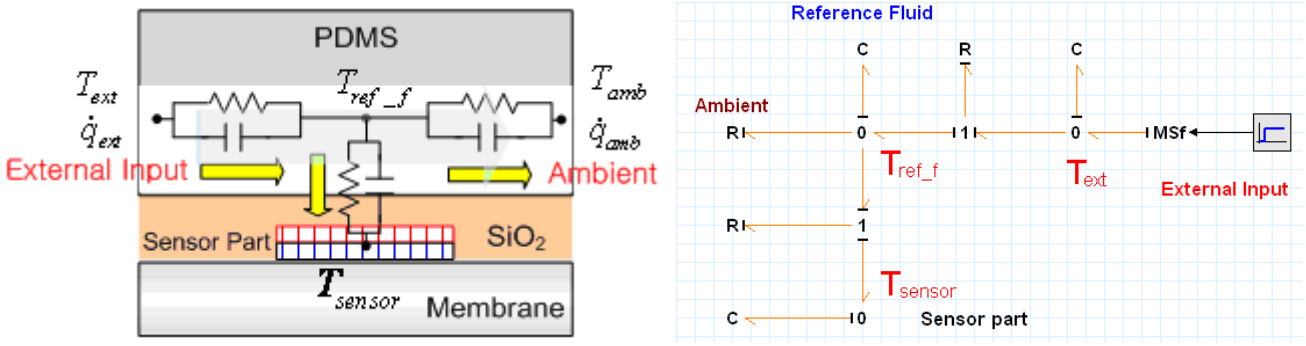

(a) (b)

Figure 14. Bond graph model of (a) a heat flux sensor part and (b) values.

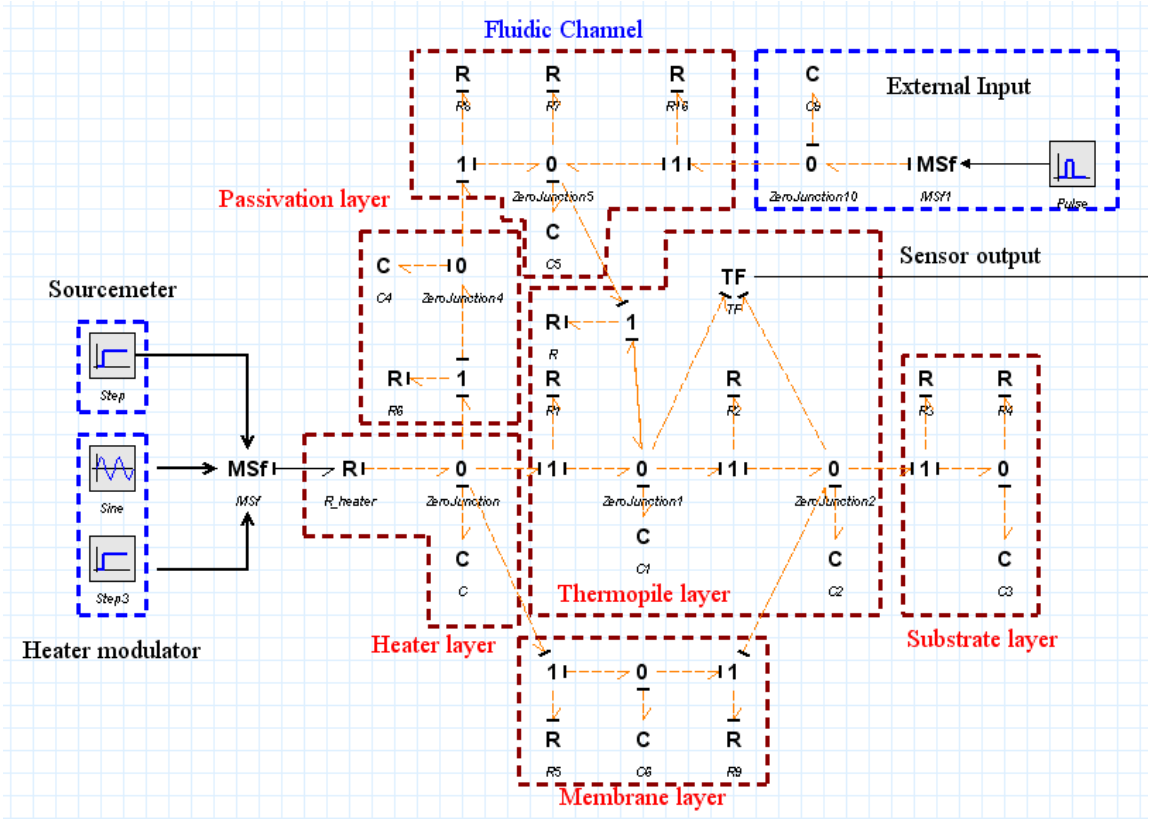

(a)

Name	Value
C1\c	4.2174e-008
C2\c	1.48e-008
C3\c	0.055528
C4\c	0.00055912
C5\c	0.002
C6\c	8.2174e-008
C7\c	2e-005
C8\c	0.0001
C9\c	0.002
C\c	1.2317e-008

Name	Value
R1\r	1500
R2\r	9090
R3\r	452.43
R4\r	6700
R5\r	1943981
R6\r	24
R7\r	6700
R8\r	800
R9\r	1943981
R\r	172.34

Name	Value
R10\r	1000
R11\r	20000000
R12\r	50
R13\r	1000
R14\r	100
R15\r	2000000
R16\r	15

(b) (Unit: C = J/K, R = K/W)

4.3. Electrical domain modeling

The electrical circuits are mainly composed mainly of electric resistors, capacitors, and operational amplifiers. Resistors and capacitors, which are the passive electrical components, can be expressed with an R_e element and a C_e element. Active electrical components, such as operational amplifier, can be developed in a bond graph model [24]. A noninverting amplifier and a lock-in amplifier can be modeled with standard elements of a bond graph and the developed bond graph model. Figure 15(a) shows an equivalent electrical circuit and lock-in amplifier; Figure. 15(b) shows the bond graph model of an electric system.

Figure 15. (a) Overall electrical circuit system; (b) Bond graph model of electrical circuit part.

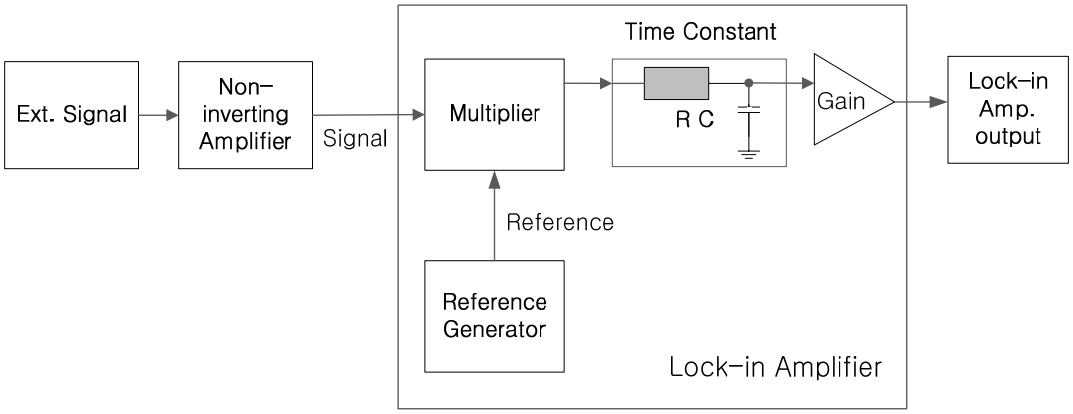

(a)

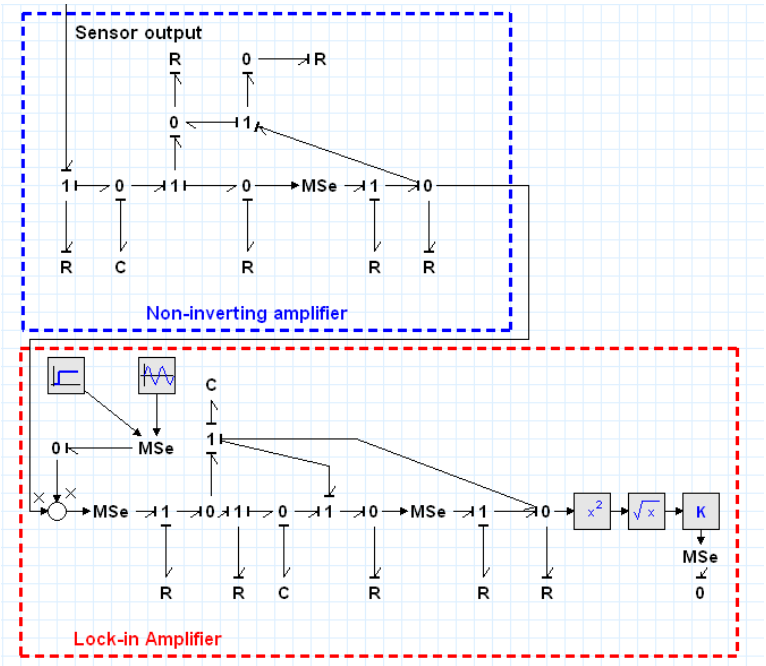

(b)

4.4. System model identification

The numerical values of the electrical and thermal parameters of the system model must be determined for simulation purposes. The values of the passive electrical components are identified from direct measurement. The manufacturer's data are used to obtain the values of the active electrical component, such as the open loop gain and the input and output resistances values.

Since the heater resistance varies with its temperature, the heat input from the heater continually changes with the resistance of the heater, even if a constant current input is applied. The relation between the resistance of the heater and the temperature is identified as per standard No. 51-1 EIA/JEDEC [31]. The sensor placed in the insulation chamber with the heating element and the heater is connected with the sourcemeter for the purpose of measuring the resistance of the heater. The resistance value of heater and the temperature of insulation chamber at equilibrium, with

increasing temperature of insulation chamber by the heating element, are recorded. The relation for this experiment is expressed as:

$$R_{heater} = 124.3 \cdot (1 - 0.0009 \cdot T)[\Omega] \quad (4)$$

The thermal parameters of the sensor were identified by means of an analytical calculation and an experimental method. The thermal parameters of the inner parts of the sensor, which consist of the thermal resistance values and the thermal capacitance values of the thermopile and membrane, were determined by numerical calculations based on both the geometry of the sensor and the thermal properties of the materials. The thermal resistance between the surface of the sensor and the ambient is determined experimentally [32]. The power is supplied to the heater in a stepwise manner with the sourcemeter. The temperature response of the sensor surface is measured with an IR thermometer. The thermal resistance is calculated with the measured temperature increment, the ambient temperature, and the measured power dissipation.

4.5. Results

The simulation results of the developed system are validated with a comparison of the experimental data. Figure 16(a) shows the measured data, and Figure 16(b) shows the simulated results with different power supplies ranging from 1.24 to 7.77 μW with the sourcemeter.

Figure 16. Comparison of the heat-flux output for calibration (input conditions: reference 7 Hz; 265 mV_{pp}; 530 mV_{Offset}; time constant 300 ms).

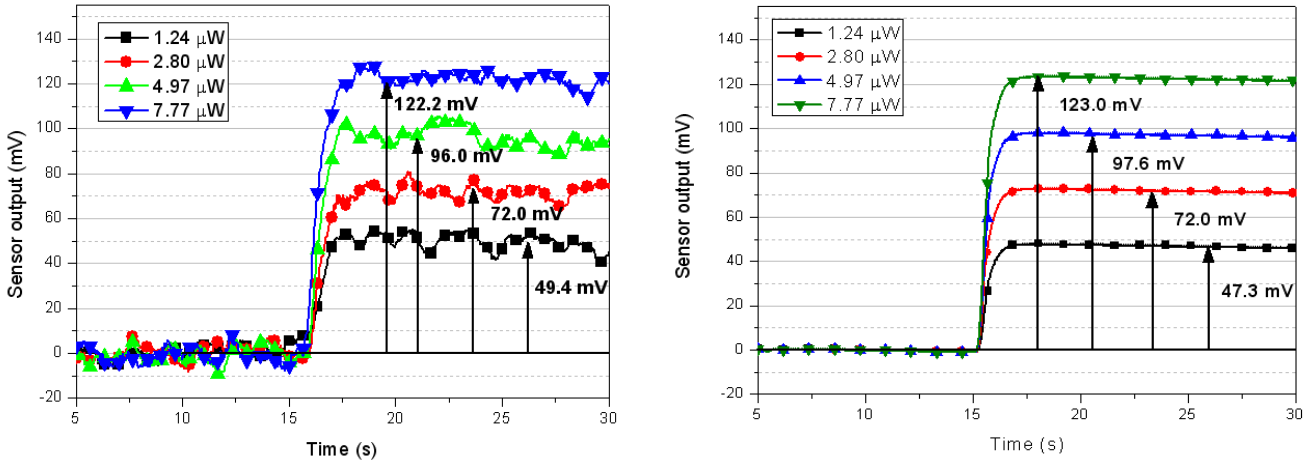

(a) Measured (b) Simulated

The experimental data has 20 mV of maximum fluctuations after reaching steady-state. This is possibly arising from the sensor geometry which has long sensitive area and that makes non-uniform temperature on it, but it is not identified yet. To compare between experimental data and simulation data, the sensor output is averaged for 10 seconds after it reaches steady-state. The simulation results follow the measured data for output voltage deviations for less than 4.2%. Figure 17 shows the Fourier transform of the sensor output signal and 20 mV of the dominant noise can be seen.

Figure. 17. Fourier transform of the sensor output signal.

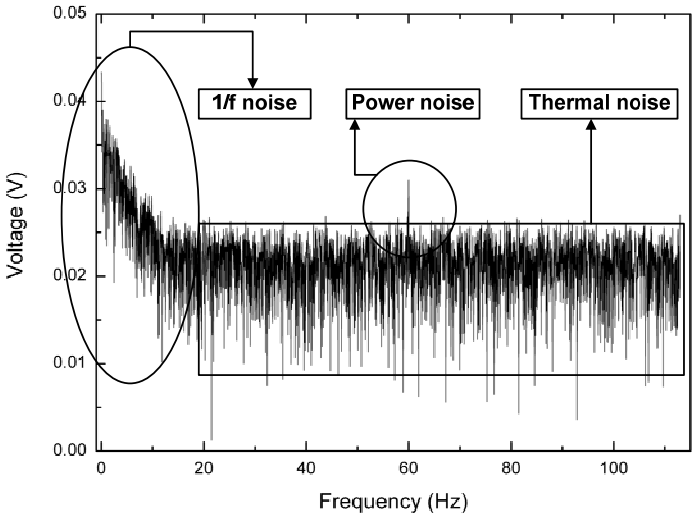

Figure 18(a) shows the measured data, and Figure 18(b) shows the simulated results with a heat supply of 14.48 to 27.64 mJ per 350 nL for the microfluidic application. The simulation results follow the measured data for output voltage deviations of less than 1% and a time constant discrepancy of 0.2 s. As it can be seen, the simulation results are in good agreement with the measured voltage responses. Because the thermal parameters of the inner part of the sensor are calculated on the basis of the geometrical dimensions, there are slight discrepancies between the measured data and the simulation data. If thermal properties of the layers are investigated in terms of the fabrication process of each test sample, the simulation model should be able to produce more accurate results. In the microfluidic application simulation, accurate measurement of the heat and velocity of the fluid can increase the accuracy of the simulation model.

Figure 18. Comparison transient response of the heat-flux output with a fluid injection (input conditions: fluid injection: 350 nL; Ambient temperature: 20.1 °C; reference flow rate: 830 nL/s).

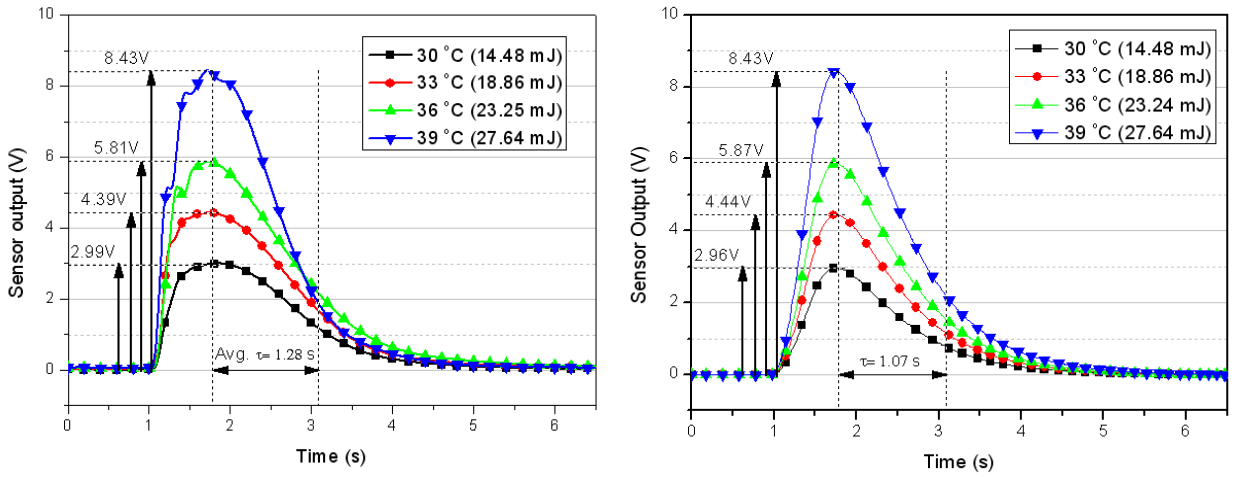

(a) Measured (b) Simulated

5. Conclusions

In this paper, we present the design and fabrication process of a microfluidic heat flux sensor. The microfluidic heat flux sensor system consists of a thermopile, a micro calibration heater, a thermistor, a PDMS fluid channel, and electronic circuits. The sensor was fabricated by a complementary-metal-oxide-semiconductor-compatible process. The characteristics of the sensing system are investigated by means of a thermal modulation method to reduce the low-frequency noise. The system has a sensitivity of 461 V/W and a resolution of 20 nW. The developed microfluidic heat flux sensor was measured with various amounts of fluidic heat to investigate the suitability of the sensor for microfluidic applications. Modeling and simulation of the electro-thermal behavior of the microfluidic heat flux sensor with an integrated electronic circuit and lock-in amplifier are presented for the purpose of designing the micro heat flux sensor system and analyzing the signal output. The proposed system model shows good agreement with the measured data.

Acknowledgements

This work was supported by the Korea Science and Engineering Foundation (KOSEF) NRL Program grant funded by the government (MEST) (No. R0A-2008-000-10065-0) and a partial support provided by Research Center for Biomolecular nano technology (RCBN).

References

1. Diller, T.E. Advances in heat flux measurement. In *Advances in Heat Transfer*, Academic Press: Boston, MA, USA, 1993; Volume 23, pp. 279-368.
2. Eminoglu, S.; Sabuncouglu Tezcan, D.; Yusuf Tanrikulu, M.; Akin, T. Low-cost uncooled infrared detectors in CMOS process. *Sensor. Actuator. A-Phys.* **2003**, *109*, 102-113.
3. Matsumiya, M.; Shin, W.; Izu, N.; Murayama, N. Nano-structured thin-film Pt catalyst for thermoelectric hydrogen gas sensor. *Sensor. Actuator. B-Chem.* **2003**, *93*, 309-315.
4. Baciocchi, M.; Bearzotti, A.; Gentili, M.; Lucchesini, A. Cu/Pd Thin-film thermopile as a temperature and hydrogen sensor. *Sensor. Actuator. A-Phys.* **1990**, *22*, 631-635.
5. Buchner, R.; Sosna, C.; Maiwald, M.; Benecke, W.; Lang, W. A high-temperature thermopile fabrication process for thermal flow sensors. *Sensor. Actuator. A-Phys.* **2006**, *130-131*, 262-266.
6. Kim, T.H.; Kim, S.J. Development of a micro-thermal flow sensor with thin-film thermocouples. *J. Micromech. Microeng*. **2006**, *16*, 2502-2508.
7. Hopper, R.H. Use of carbon micro-particles for improved infrared temperature measurement of CMOS MEMS devices. *Meas. Sci. Technol*. **2010**, *21*, 045107.
8. Johannessen, E.A.; Waver, J.M.R.; Cobbold, P.H.; Cooper, J.M.A. Suspended membrane nanocalorimeter for ultralow volume bioanalysis. *IEEE Trans. Nanobiosci*. **2002**, *1*, 29-36.
9. Giraldo-Gutierréz, L.; Moreno-Piraján, J.C. Determination of the temperature change by means of an outcoming signal of electric resistance in an isoperibolic calorimetric cell. Obtainment of heat solution. *Sensors* **2005**, *5*, 633-643.
10. Kao, P.H.; Shih, P.J.; Dai, C.L.; Liu, M.C. Fabrication and characterization of CMOS-MEMS thermoelectric micro generators. *Sensors* **2010**, *10*, 1315-1325.

11. Maskow, T.; Harms, H. Real time insights into bioprocesses using calorimetry: State of the art and potential. *Eng. Life Sci.* **2006**, *6*, 266-277.
12. Macfarlane, G.G. A Theory of contact noise in semiconductors. *Proc. Phys. Soc. B* **1950** , *63*, 807-814.
13. Randjelović, D.; Petropoulos, A.; Kaltsas, G.; Stojanović, M.; Lazić, Ž.; Djurić Z.; Matić, M. Multipurpose MEMS thermal sensor based on thermopiles. *Sensor. Actuator. A-Phys.* **2008**, *141*, 404-413.
14. Oh, S.H.; Lee, K.C.; Chun, J.; Kim, M.H.; Lee, S.S. Micro heat flux sensor using copper electroplating in SU-8 microstructures. *J. Micromech. Microeng*. **2001**, *11*, 221-225.
15. Oh, S.H.; Lee, S.H.; Jeon, J.C.; Kim, M.H.; Lee, S.S. Bulk-micromachined circular foil type micro heat-flux sensor. *Sensor. Actuator. A-Phys.* **2006**, *132*, 581-586.
16. Zhang, Y.; Tadigadapa, S. Calorimetric biosensors with integrated microfluidic channels. *Biosens. Bioelectron*. **2004**, *19*, 1733-1743.
17. Baier, V.; Födisch, R.; Ihring, A.; Kessler, E.; Lerchner, J.; Wolf, G.; Köhler, J.M.; Nietzsch, M.; Krügel, M. Highly sensitive thermopile heat power sensor for micro-fluid calorimetry of biochemical processes. *Sensor. Actuator. A-Phys.* **2005**, *123-124*, 354-359.
18. Dehé A.; Fricke, K.; Hartnagel, H.L. Infrared thermopile sensor based on AlGaAs-GaAs micromachining. *Sensor. Actuator. A-Phys.* **1995**, *46-47*, 432-436.
19. Johannessen, E.A.; Weaver, J.M.R.; Cobbold, P.H.; Cooper, J.M. Heat conduction nanocalorimeter for pl-scale single cell measurements. *Appl. Phys. Lett*. **2002**, *80*, 2029-2031.
20. Kemp, R.B.; Guan, Y. Heat flux and the calorimetric-respirometric ratio as measured of catabolic flux in mammalian cells. *Thermochim. Acta.* **1997**, *300*, 199-211.
21. Olmo, E. Nucleotype and cell size in vertebrates: A review. *Basic Appl. Histochem.* **1983**, *27*, 227-256.
22. Paynter, H.M. *Analysis and Design of Engineering Systems.* The MIT Press: Cambridge, MA, USA, 1961.
23. Karnopp, D.; Rosenberg, R. *Analysis and Simulation of Multiport Systems*. The MIT Press: Cambridge, MA, USA, 1968.
24. Granda, J.J. The role of bond graph modeling and simulation in mechatronics systems-an integrated software tool: CAMP-G, MATLAB-SIMULINK. *Mechatronics* **2002**, *12*, 1271-1295.
25. Thoma, J.U. Bond graphs for thermal energy transport and entropy flow. *J. Franklin Inst-Eng. Appl. Math*. **1971**, *292*, 109-120.
26. Pal, S.K.; Linkens, D.A. Temperature distribution in steel during hot rolling: pseudo-bond graph view. *Simul. Modell. Practice Theory* **2002**, *10*, 68-85.
27. Kim,S.M.; Lee, S.K. Prediction of thermo-elastic behavior in a spindle-bearing system considering bearing surroundings. *Int. J. Machine Tools Manuf.* **2001**, *41*, 809-831.
28. Kim, J.K.; Nakayama, W.; Ito, Y.; Shin, S.M.; Lee, S.K. Estimation of thermal parameters of the enclosed electronic package system by using dynamic thermal response. *Mechatronics* **2009**, *19*, 1034-1040.
29. 20-sim program. Available online: http://.20sim.com/ (accessed on 16 October 2007).
30. Incropera, F.P.; DeWitt, D.P.; Bergman, T.L.; Lavine, A.S. *Fundamentals of Heat and Mass Transfer.* Wiley: Hoboken, NJ, USA, 2006.

31. JEDEC. *Integrated Circuits Thermal Measurement Method-Electrical Test Method (Single Semiconductor Device).* EIA/JESD Standard. **1995**, *51*, 3-23.
32. Kim, J.K.; Kim, T.H.; Cho, S.C.; Shin, S.M.; Lee, S.K. Modeling and fabrication of thin film thermopile sensor. *J. Vac. Sci. Technol. B* **2009**, *27*, 1466-1472.